Chemical Engineering Journal 515 (2025) 162709

Contents lists available at ScienceDirect

Chemical Engineering Journal

journal homepage: www.elsevier.com/locate/cej

Reactive extrusion recycling of polymethyl methacrylate to methyl methacrylate and methacrylic acid

Yanfa Zhuang [a], Tien Dat Nguyen [a], Mahdi Sharifian [a], Jean-Luc Dubois [b], Abdellah Ajji [a], Gregory Patience [a,*]

[a] Polytechnique Montreal, Dept. Chemical Engineering, CP 6079, Succ CV, Montreal, Québec H3C 3A7, Canada
[b] Trinseo France SAS - Altuglas International SAS, Tour CB21, 16 place de l'Iris, Courbevoie, 92400, France

ARTICLE INFO

Keywords:
Polymethyl methacrylate
Methyl methacrylate
Methacrylic acid
Plastic recycling
Reactive extrusion
Hydrolysis extrusion

ABSTRACT

The global production of polymethyl methacrylate (PMMA) reached 4 million tonnes annually, yet only 10% of PMMA, primarily post-industrial scraps, is recycled. Recycling end-of-life PMMA, which often contains additives or composite components, poses challenges in achieving crude methyl methacrylate (MMA) monomer with comparable purity to post-industrial scraps. Hydrolyzing end-of-life PMMA presents a viable alternative to produce methacrylic acid (MAA) and simplifies the purification process of crude MMA. However, current PMMA hydrolysis is limited to lab-scale and batch operations in fluidized/fixed beds and stirred tank reactors. In this study, we demonstrate a pilot-scale, two-stage reactive hydrolysis extrusion system for the continuous conversion of injection- and extrusion-grade PMMA scraps into MMA and/or MAA at 330 °C to 370 °C. Residence time distribution (RTD) tests characterized the hydrodynamics of the screw configuration for PMMA extrusion, revealing that lower screw speed and feeding rate increase reaction time. A Plackett-Burman design identified temperature and catalyst type as significant factors for MMA hydrolysis. Under optimized conditions, hydrolysis extrusion without any catalysts achieved the highest MMA yield of 89% and 96% PMMA conversion. Hydrolysis extrusion with 10% H-type zeolite Y with an SiO_2/Al_2O_3 ratio of 80 at 370 °C resulted in a 5.3% MAA yield, a 67% MMA yield, and near-complete PMMA conversion. Liquid acid catalysts directly hydrolyzed PMMA to poly(MMA-co-MAA) copolymer and/or PMAA, followed by dehydration of two adjacent acid groups to form six-member glutaric anhydride. KOH solution hydrolyzed PMMA to poly(MMA-co-MAA) and/or PMAA potassium salt.

1. Introduction

Industry produces 400 million tonnes of plastic waste annually [1], with only 10% being recycled [2]. Over 80% of plastic waste is either trashed in landfills, incinerated, or discarded into the environment [3], creating a critical environmental crisis. Commercially used plastics contain various additives, such as colorants, flame retardants, plasticizers, and antioxidants [4]. These additives increase risks to environmental organisms and complicate the recycling process.

Polymethyl methacrylate (PMMA), also known as acrylic glass, Plexiglas, Perspex, and Altuglas, is an optically transparent, lightweight thermoplastic with good impact strength, excellent weather resistance, and scratch resistance [5,6]. Annually, the industry produces around 4 million tonnes of PMMA for optical, electronic, and construction applications, but only 10% of PMMA is collected to be recycled in the EU. Most waste PMMA is incinerated or landfilled [7]. Recycled PMMA predominantly comes from post-industrial cast sheets, extrusion sheets, or injection molded parts, which can be mechanically recycled into new PMMA products or thermolyzed into high-purity regenerated MMA (r-MMA) [6]. End-of-life PMMA containing additives or composite components requires chemical recycling, but producing r-MMA of similar purity as post-industrial PMMA scraps is more challenging.

Thermolyzing PMMA above 350 °C in an inert atmosphere yields 70% to 90% monomer at over 90% r-MMA purity [8]. PMMA depolymerization follows a radical reaction mechanism [9,10]. Commercial reactors, include molten metal baths, fluidized beds, reactive twin-screw extruders, augers, rotating drums, dry distillation stills, rotating paddles, and stirred tank reactors [9–11]. Fillers or additives such as metals, glass fibers, granite, and colorants in end-of-life PMMA lower monomer yield and introduce impurities, increasing purification costs in downstream processing [12,13]. Crude r-MMA may contain oligomers and impurities like methyl acrylate, ethyl acrylate, methyl

* Corresponding author.
E-mail address: gregory-s.patience@polymtl.ca (G. Patience).

https://doi.org/10.1016/j.cej.2025.162709
Received 23 December 2024; Received in revised form 30 March 2025; Accepted 15 April 2025
Available online 14 May 2025

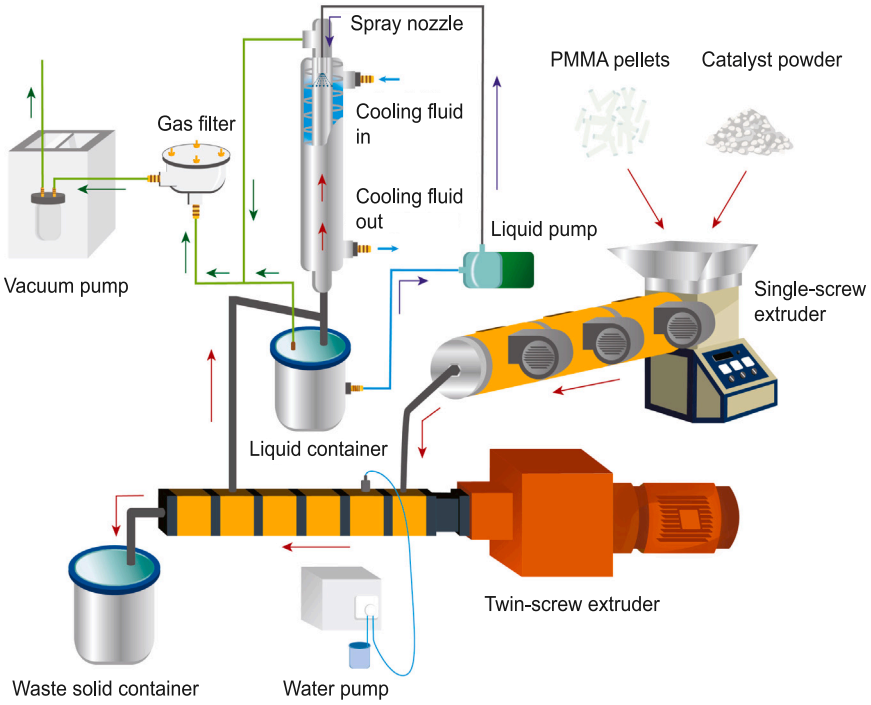

Fig. 1. Setup of the two-stage reactive extrusion hydrolysis system. The single screw extruder was connected to the twin-screw extruder, functioning as a feeder. A vacuum degassing and circulation condensation system was employed to collect the liquid products.

pyruvate, methyl or ethyl propionate, methyl isobutyrate, methyl 2-methylbutyrate, and pentanedioic acid, 2,4-dimethyl-, monomethyl ester [14–16]. Some impurities have close boiling points (BP) or molecular structures to MMA, complicating the separation and purification of crude r-MMA. For instance, ethyl acrylate has a boiling point almost identical to MMA (100 °C vs. 101 °C) and an odor threshold over 20 times lower than MMA [17,18]. Crude r-MMA recycled from low-quality scraps with more impurities requires higher purification costs, and some impurities remain difficult to eliminate completely. This limits the application of r-MMA in strictly regulated markets for producing high-quality PMMA products.

To reduce the downstream purification costs of crude r-MMA generated from low-quality end-of-life PMMA, Chub et al. [12,19] proposed a new route to convert PMMA into methacrylic acid (MAA) instead of MMA. MAA has a boiling point of 162 °C and many other different physico-chemical properties [20], which makes it easier to separate from the liquid products. The purified MAA can then be converted into MMA as a monomer or sold as a specialty chemical.

MAA, a colorless carboxylic acid with a pungent odor, is mainly used as co-monomer in paints, adhesives, leather treatment, fiber processing, and as a rubber modifier [21]. It is also used as a precursor to synthesize its esters (MMA), copolymers with other monomers, and MAA salts [22]. The market size for MAA, other than as an intermediate, is approximately 10% of the MMA market. New MMA plants using ethylene as a feedstock are expected to come online in the coming years. These plants do not coproduce MAA, which will further increase the interest in MAA.

Industrial MAA production primarily relies on the acetone–cyanohydrin (ACN) process and the oxidation of isobutylene or ethylene-based methacrolein [22,23]. HCN and cyanide intermediates are the major feedstocks for the ACN process, while alternative oxidation routes consume substantial amounts of fossil-fuel-derived feedstocks. The industrial viability of greener production methods, such as converting biomass-derived citric acid or citramalic acid to MAA via decarboxylation and dehydration at 250 °C [24], are hindered by low yields and poor atom economy [22,25]. The economic benefits of producing MAA from PMMA scraps are substantial. This process not only facilitates the management of larger volumes of PMMA waste but also aligns the market demand for MAA with the available supply of PMMA waste. Additionally, the BP and melting points (MP) of the involved compounds facilitate purification compared to PMMA thermolysis to MMA. For instance, methyl isobutyrate (BP 90 °C) hydrolyzes to isobutyric acid (BP 155 °C, MP −47 °C), and ethyl acrylate (BP 100 °C) hydrolyzes to acrylic acid (BP 141 °C), both of which can be easily separated from MAA (BP 162 °C, MP 15 °C) [26].

Current recycling of PMMA to MAA is constrained to lab-scale fluidized/fixed bed reactors [12,19,27] and stirred tank reactors [6,28]. The primary reaction mechanism involves a series of steps where PMMA is thermally depolymerized into MMA, which is subsequently hydrolyzed into MAA. However, the acidic solid catalysts used in this process deactivate after each batch reaction. To date, continuous recycling of PMMA into MAA has not been reported.

In fixed-bed [27] and fluidized-bed [12,19] reactors, previous studies have tested only gram-scale quantities of virgin PMMA powder, achieving an MAA yield of over 50% without accounting for energy consumption or unit recycling costs. In stirred-tank reactors [6,28], researchers primarily used waste artificial marble containing 40% PMMA and 60% aluminum hydroxide ($Al(OH)_3$) to recover MMA and MAA, with MMA as the dominant product. However, stirred-tank processes operate in batch mode, necessitating downstream reactor cleaning, which could lead to high operational costs in industrial applications.

Reactive extrusion, which combines conventional physical melt extrusion with chemical reactions in a single screw or twin-screw extruder, is a promising method to produce continuously crude r-MMA from scraps [10,29]. The European project MMAtwo demonstrated a continuous reactive extrusion thermolysis process, converting extrusion, injection, and cast grade scraps into MMA monomer with yields between 80% and 90% at the pilot scale [30].

In this study, we developed a pilot-scale two-stage reactive extrusion hydrolysis system (Fig. 1) to convert injection- and extrusion-grade scraps into MMA and/or MAA from 330 °C to 370 °C. The first-stage single screw extruder served as a feeder, injecting melt into the second-stage twin-screw extruder where it degraded further. The designed intermeshing co-rotating twin-screw extruder provides self-cleaning

capabilities, enabling the efficient extrusion of unreacted residues and solid catalysts [29]. We injected a fluorescent tracer to study the residence time distribution (RTD) of PMMA melt along the twin-screw extruder. Additionally, we applied a Plackett-Burman design to identify the optimal conditions for degradative extrusion before further optimizing operational parameters [31]. Both multiphase extrusion using solid powder catalysts (H-type zeolite Y-80 and gamma Al_2O_3) and homogeneous extrusion with liquid catalysts (KOH, H_2SO_4, and phosphotungstic acid hydrate (PTA) solutions) were investigated. We compared two degassing methods: vacuum and atmospheric degassing. MMA was the predominant condensed product, regardless of the presence of steam and/or catalyst. Notably, multiphase extrusion of PMMA with zeolite Y-80 at 370 °C converted almost all the PMMA but the yield to MAA was only 5.3% when a single catalyst was used to recycle injection-grade scraps.

2. Experimental

2.1. Materials

Injection-grade PMMA scraps and extrusion-grade PMMA scraps were provided by Montreal Polymers. Virgin PMMA granules (M_w = 100 000 g mol^{-1}) were supplied by Altuglas. We purchased gamma Al_2O_3 (PURALOX SCCa-5/200) from Sasol and H-type zeolite Y (CBV780, SiO_2/Al_2O_3 mole ratio = 80, 780 m g^{-2}) powder from Zeolyst. Phosphotungstic acid hydrate (PTA) was obtained from Thermo Scientific Chemicals. Isopropyl alcohol (≥99.8%, GC grade) and GC–MS calibration standard MAA (99% with 250 ppm MEHQ as inhibitor), methanol (≥99.9%, HPLC grade), and acetone (≥99.9%, HPLC grade) were sourced from Sigma-Aldrich. MMA (≥99.6% with 6-tert-Butyl-2,4-xylenol) was purchased from TCI America. Anhydrous ethanol (HPLC grade) was provided by Commercial Alcohols. Potassium hydroxide (reagent grade, 90%) and the fluorescent tracer anthracene were also purchased from Sigma-Aldrich. Sulfuric acid (70% w/w) was obtained from Anachemia, and solvent acetone (≥99.6%, ACS reagent) was sourced from Thermo Scientific Chemicals.

2.2. Characterization

2.2.1. N_2 adsorption

A Quantachrome Autosorb-1 analyzer characterized the surface area and porosity of the gamma Al_2O_3 catalyst. The Al_2O_3 powder was vacuum degassed at 350 °C for 12 h. The specific surface area of Al_2O_3 was determined using the multi-point Brunauer-Emmett-Teller (BET) method in the P/P_0 range of 0.05 to 0.30 [32]. The adsorbed N_2 volume at $P/P_0 = 0.99$ was used to estimate the total pore volume. The t-plot method in the t range of 3.5 Å to 5.0 Å was used to determine the volume of micropores and the specific surface area of mesopores. The average pore size and pore size distribution were estimated using the Barrett–Joyner–Halenda (BJH) model [32].

2.2.2. Particle size distribution (PSD)

A Horiba LA950 laser diffractometer measured the particle size distribution (PSD) of the powder.

2.2.3. Scanning electron microscopy with energy dispersive X-ray spectroscopy (SEM/EDS)

A small piece of the extrudate was cut using pliers. The cut section, created by the pliers, was oriented upward for SEM analysis. Prior to scanning, a thin layer of gold (Au) was sputter-coated onto the sample surface to enhance conductivity. The morphology and elemental mapping of the extrudes were analyzed using a JEOL JSM-7600F Scanning Electron Microscope (SEM) equipped with a Schottky field emission gun and an Oxford Instruments X-MaxN Energy Dispersive Spectroscopy (EDS) detector.

2.2.4. Fourier-transform infrared spectroscopy (FTIR)

A PerkinElmer Spectrum 65 FTIR spectrometer detected the functional groups of PMMA extrudates and scraps. The solid extrudates and scraps were dissolved in acetone and kept at room temperature for 12 h. The supernatant was separated and dropped onto the surface of the spectrometer's sample chamber. After the acetone evaporated, a thin film formed on the chamber surface. The spectrometer then scanned the film from 4000 to 600 cm^{-1}.

2.2.5. Gel permeation chromatography (GPC)

The molecular weight (Mw) of PMMA scraps was measured with a Thermo Scientific UltiMate 3000 HPLC system equipped with two tandem Shodex GPC columns, KF-803L and KF-804L. The system was calibrated with the Shodex PMMA calibration kit, STANDARD M-75. The GPC system utilized a Refractive Index (RI) detector and tetrahydrofuran (THF) as the eluent. The temperature of the RI detector and the columns was maintained at 35 °C, and the eluent flow rate was kept at 1 mL min^{-1}. All PMMA scraps were dissolved in THF prior to injection.

2.2.6. Thermogravimetric analysis (TGA)

Thermogravimetric degradation curves of PMMA scraps and extrudates were determined using a TA Instruments Q500 or Q550 Thermogravimetric Analyzer. All samples were heated from room temperature to 700 °C at a rate of 5 °C min^{-1} under a nitrogen atmosphere with a flow rate of 60 mL min^{-1}.

2.2.7. Differential scanning calorimetry (DSC)

The glass transition temperature (T_g) of PMMA scraps was measured using a TA Instruments DSC Q-2000 differential scanning calorimeter. The samples, encapsulated in aluminum pans, were kept at 135 °C for 10 min to eliminate thermomechanical history, followed by cooling to 40 °C. Each sample was heated to 180 °C at a rate of 10 °C min^{-1} and then cooled to 40 °C under a nitrogen atmosphere with a flow rate of 50 mL min^{-1}. This heating and cooling cycle was repeated three times, with the second heating cycle used to plot the DSC curve.

2.3. Liquid products analysis

The liquid products were quantitatively and qualitatively analyzed using an Agilent 7890A/5975C Gas Chromatography-Mass Spectrometry (GC–MS) system equipped with an Agilent 7693 Autosampler. A 30-meter Agilent J&W DB-Wax UI column (polyethylene glycol stationary phase) with an inner diameter of 0.25 mm and a film thickness of 0.25 μ m was used to separate the components. For qualitative analysis, the MSD scanned the m/z ratio in the range of 29 to 500 in full scan mode. For quantitative analysis, selected ion monitoring (SIM) mode was employed to scan acetone (m/z = 43 and 58), methanol (m/z = 31), MMA (m/z = 41, 69, and 100), and MAA (m/z = 41 and 86). The concentration of the four components was quantified using an external calibration method. Anhydrous ethanol was used as the solvent for all calibration standards and samples.

The PMMA conversion (X_{PMMA}), product selectivity (S_i), and yield (Y_i) were calculated using the following formulas:

$$X_{PMMA} = \left(1 - \frac{\text{mass of extrudates - catalyst fed}}{\text{mass of PMMA fed}}\right) \times 100\% \quad (1)$$

$$S_i = \frac{\text{moles of product i} \times \text{carbon number in producti}}{\text{MMA moles in degraded PMMA} \times 5} \times 100\% \quad (2)$$

$$Y_i = \frac{\text{moles of product i} \times \text{carbon number in product i}}{\text{MMA moles in PMMA fed} \times 5} \times 100\% \quad (3)$$

where i means different liquid products (i.e. MMA, MAA, MeOH and acetone).

To simplify the calculation of PMMA conversion, we assume that the extrudates consist solely of unreacted PMMA and catalysts. This assumption holds despite the presence of additional components such as carbon deposits and partially hydrolyzed PMMA in the extrudates. However, PMMA remains the predominant polymer residue in the extrudates.

2.4. Experimental set-up

PMMA scraps or PMMA scrap-solid catalyst blends were fed into a two-stage extruder system (Fig. 1). The first-stage was an SJ30 single screw extruder (diameter D = 30 mm, length to diameter ratio L/D = 25:1) with three heating zones, manufactured by Zhangjiagang MC Machinery Co., Ltd. The second-stage was a T20 co-rotating twin-screw extruder (D = 22.4 mm, L/D = 46:1) manufactured by Nanjing Huaju Machinery Co., Ltd. The temperature was set to 220 °C at the entrance and rose to 330 °C for Temperature Profile I and 370 °C for Temperature Profile III Fig. 4.

The screw configuration of the twin-screw extruder consists of a feeding zone, liquid injection zone, reaction zone, degassing zone, and compression zone (Supplementary Fig. A.1). Two reverse conveying screw elements were configured separately before the liquid injection zone and the degassing zone to build melt pressure. An AZURA P 4.1S pump injected liquid from the third barrel of the second-stage extruder. A 304 stainless steel AB double-wall fin heat exchanger (L = 0.975 m, D = 0.05 m) condensed the condensable gaseous products from the degassing port. A 304 stainless steel vacuum container connected to the bottom of the heat exchanger collected condensed products, while another vacuum container collected residues from the die of the second-stage extruder. To aid in the condensation of products, a magnetic drive water circulating pump transported liquid from the liquid container to a spray nozzle placed at the top of the heat exchanger.

During the vacuum degassing process, a vacuum pump was applied to the condenser and the liquid container. The vacuum pump was removed for the atmospheric degassing process.

PMMA exhibits low viscosity above 300 °C. In the designed screw and barrel configuration (Supplementary Fig. A.1), the second barrel (feeder barrel) is set at 220 °C, ensuring that PMMA behaves as a viscous polymer. To prevent backflow of gas and melt, we incorporated reverse screw elements before the liquid injection zone, creating a choked zone.

The third to fifth barrels constitute the reaction zone, where PMMA melt transitions to a low-viscosity, water-like state. In these zones, shear forces primarily serve to renew material surfaces and enhance mixing. However, the depolymerization and hydrolysis reactions in this system are primarily driven by heat rather than shear forces.

From the degassing zone to the final compression zone (sixth and seventh barrels), the temperature is maintained at or below 250 °C, where shear forces facilitate the extrusion of unreacted materials. The reaction barrels operating above 330 °C involve a degradative reactive extrusion process, significantly reducing polymer viscosity.

Although PMMA exhibits low viscosity and a water-like flow behavior above 330 °C, we still consider it to be in a melt state. The generated monomers, MMA and MAA, transitions to the gas phase above 300 °C. The designed reaction system constitutes a complex heterogeneous system involving melt-solid-gas interactions.

2.5. Experimental procedure

The PMMA feeding rate corresponded to the screw rotation speed of the single screw extruder. Blends of PMMA scraps and powder catalysts, or PMMA scraps alone, were fed from the hopper into the first-stage extruder. The melt was then transferred into the second barrel of the second-stage extruder. To avoid severe PMMA melt degradation before the liquid injection zone, the three heating zones on the first-stage extruder were maintained at 200 °C, and the connector between the two stages of the extruder, and the second barrel of the twin-screw extruder were kept at 220 °C.

A liquid pump injected liquid from the third barrel of the twin-screw extruder during the melt extrusion process. PMMA depolymerization/hydrolysis commenced from the third to the sixth barrels. The last barrel (i.e., the seventh barrel) of the twin-screw extruder was kept at 220 °C to terminate the PMMA depolymerization and extrude the residues. The operating temperature (250 °C or 300 °C) of the degassing barrel was lower than the reaction temperature (330 °C, 350 °C or 370 °C) in the third to fifth barrels.

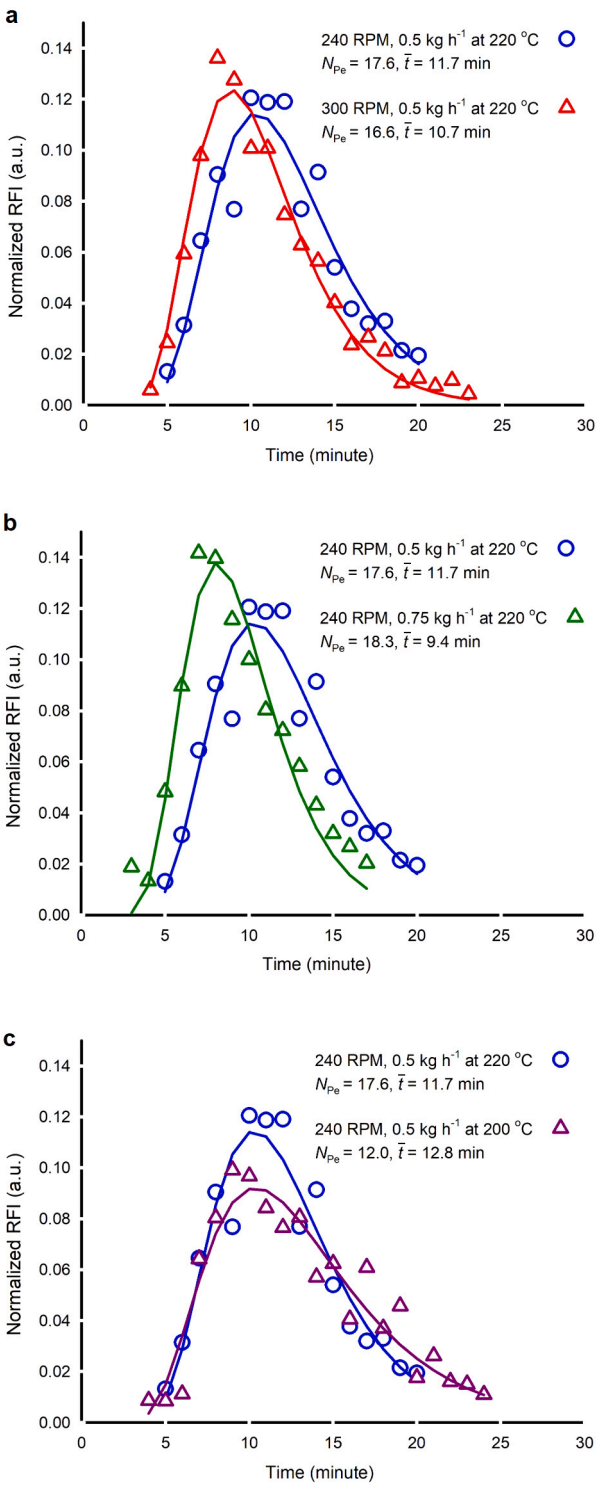

Fig. 2. Residence time distribution (RTD) of reaction zones in a twin-screw extruder. The hollow symbols represent normalized relative fluorescence intensity (RFI) curves, while the solid lines are the simulated RTD curves using the axial dispersion model. N_{Pe} denotes the Peclet number, and $\bar{t}$ represents the mean residence time. **a**, Normalized RTD at different screw speeds for a feeding rate of 0.5 kg h^{-1} at 220 °C. **b**, Normalized RTD at different feeding rates at 240 rpm and 220 °C. **c**, Normalized RTD at different extrusion temperatures for a feeding rate of 0.5 kg h^{-1} at 240 rpm.

The third to fifth barrels constitute the reaction zone, where PMMA melt transitions to a low-viscosity, water-like state.

The rotation speed of the twin-screw extruder was maintained at 240 rpm, 300 rpm, or 360 rpm. A chiller set at 3.5 °C cooled the condenser. The collection of hydrolyzed or thermolyzed products began once the reaction temperature was reached. Each trial was conducted for 1 h. The feeding rate for each trial was either 0.5 kg h^{-1} or 0.75 kg h^{-1}.

For the DOE tests, 1.5 L of a 20:80 (L:L) ethanol–water solution was added to the liquid container to generate a spray prior to reaction. For reactions under optimized operating conditions, 1 L of pure ethanol was used in the liquid container to form a spray and absorb condensable gaseous components. Residues from the die of the twin-screw extruder were weighed to calculate PMMA conversion. Liquid in the container was collected and analyzed by GC–MS.

2.6. Residence time distribution (RTD) measurement

During the extrusion of virgin PMMA, 0.1 g of the fluorescent tracer anthracene was injected at the position of the liquid injector (Supplementary Fig. A.1a). Extrudates were collected every minute and subsequently dissolved in a mixture of isopropyl alcohol and acetone in a 3:2 ratio (L:L). The fluorescence of the PMMA solutions, placed in a 384-well plate, was quantitatively measured using a TECAN Spark multimode microplate reader. The monochromator was set to an excitation wavelength of 397 nm and an emission wavelength of 352 nm.

We characterized the hydrodynamics with an axial dispersion model to fit [33,34]:

$$\frac{\partial C}{\partial \theta} + \frac{\partial C}{\partial \xi} = \frac{1}{N_{\mathrm{Pe}}} \frac{\partial^2 C}{\partial^2 \xi} \tag{4}$$

where C is the normalized relative fluorescence intensity (RFI), $\theta = tu/Z$ is the non-dimensional time, $u = Q/A$ is the melt velocity, Q is the melt volume feeding rate, and A is the internal cross-sectional area of the die, Z is the extrusion length (0.773 m), $\xi = z/Z$ is the non-dimensional length, Pe is the dimensionless Peclet number defined as $N_{\mathrm{Pe}} = uZ/D$, and D is the axial dispersion coefficient.

The injection of the fluorescence tracer is considered to be in the form of a bolus pulse. The exact analytic solution for the bolus pulse function is [33]:

$$G'(\theta) = G(\theta) - H(\theta - \tau)G(\theta - \tau) \tag{5}$$

$$H(\theta - \tau) = \begin{cases} 0, \theta \le \tau \\ 1, \theta > \tau \end{cases} \tag{6}$$

$$G(\theta) = 0.5 \left[\mathrm{erfc}\sqrt{\frac{N_{\mathrm{Pe}}}{4\theta}}(1-\theta) + e^{N_{\mathrm{Pe}}}\mathrm{erfc}\sqrt{\frac{N_{\mathrm{Pe}}}{4\theta}}(1+\theta) \right] \tag{7}$$

where, $\tau = t_d u/Z$ is the non-dimensional time length of the pulse injection, and t_d is the delay time from tracer injection to the first extrusion. Tracer was injected from the liquid injector position (Supplementary Fig. A.1a).

For the pulse injection, the mean residence time ($\bar{t}$) can be expressed in both continuous and discrete forms as follows [35]:

$$\bar{t} = \frac{\int_0^\infty tC(t)dt}{\int_0^\infty C(t)dt} = \frac{\sum t_i C_i \Delta t_i}{\sum C_i \Delta t_i} \tag{8}$$

where, Δt_i is 1 min, as samples were collected at 1 min intervals.

We normalized the relative fluorescence intensity (RFI) data and the model to ensure that the area under the curves equals one:

$$Y_i = \frac{C_i}{\sum C_i \Delta t} \tag{9}$$

$$\sum Y_i = 1 \tag{10}$$

The Peclet number characterizes the extrusion hydrodynamics by determining the number of continuous stirred tank reactors (CSTRs) in series [33]:

$$N_{\mathrm{CSTR}} = \frac{N_{\mathrm{Pe}}}{2} + 1 \tag{11}$$

Table 1
Factors and levels selection for design of experiments (DOE)

No.	Factor	Level 1	Level 2
Factor 1	T (°C)	330	350
Factor 2	N_{TSE} (rpm)	240	360
Factor 3	Q_{PMMA} (g h^{-1})	500	750
Factor 4	Scrap	Injection	Extrusion
Factor 5	Catalyst	HY(80)	Al_2O_3

Note: T-temperature, N_{TSE}-screw rotation speed of twin-screw extruder, Q_{PMMA}-PMMA scrap feeding rate.

Table 2
Plackett–Burman design including five factors at two levels.

Run	Block	T °C	N_{TSE} rpm	Q_{PMMA} g h^{-1}	Scrap	Catalyst
1	1	350	240	0.75	Injection	Al_2O_3
2	1	330	240	0.5	Injection	Al_2O_3
3	1	350	360	0.5	Extrusion	Al_2O_3
4	1	350	360	0.5	Extrusion	HY(80)
5	1	330	240	0.75	Extrusion	HY(80)
6	1	350	360	0.75	Injection	HY(80)
7	1	330	360	0.5	Injection	Al_2O_3
8	1	330	240	0.5	Extrusion	HY(80)
9	1	330	360	0.75	Injection	HY(80)
10	1	350	240	0.75	Extrusion	Al_2O_3
11	1	330	360	0.75	Extrusion	Al_2O_3
12	1	350	240	0.5	Injection	HY(80)

Note: The catalyst constitutes 1.8% by weight of the PMMA scraps. The rate of H_2O injection is set to 1.2 times the theoretical amount required for the reaction converting MMA to MAA and methanol.

2.7. Design of experiments (DOE)

To determine the optimal reaction operating conditions, we employed a Plackett-Burman design with five factors, each evaluated at two levels (Table 1).

The Plackett-Burman design (Table 2) consists of 12 unique runs without any repetitions. The experimental results were analyzed using Minitab Statistical Software 22 (trial version). To analyze the factorial design, the categorical factors scrap type (factor 4) and catalyst type (factor 5) were assigned low values of −1 (injection, Al_2O_3) and high values of 1 (extrusion, HY(80)).

Vacuum degassing improves efficiency and is widely used in devolatilization during polymer extrusion. However, MMA water vapor mist that forms in the condensation and collection steps reduces yield. Therefore, we excluded degassing type as a factor in the DOE.

3. Results and discussion

3.1. Residence time distribution (RTD) test and modeling

Screw speed, feeding rate, temperature, and screw profile affect the mixing pattern and residence time distribution (RTD) within a twin-screw extruder. Increasing screw speed or decreasing feeding rate reduces the fill fraction of materials in the extruder [36]. A lower degree of fill enhances axial mixing within the extruder, as evidenced by the N_{Pe}. N_{Pe}, the reciprocal of the dispersion number, quantifies the extent of axial mixing or backmixing [35,37]. A lower N_{Pe} indicates increased backmixing. Conversely, a higher N_{Pe} corresponds to greater plug flow behavior and reduced interactions between degradation products and PMMA. This condition helps minimize selectivity towards certain impurities, such as isobutyrate. Controlling N_{Pe} in the extruder is crucial for optimizing the balance between mixing to achieve uniformity and minimizing backmixing to maintain product quality.

A fluorescence tracer was introduced at the liquid injector port (Supplementary Fig. A.1a). Increasing the screw speed from 240 rpm to 300 rpm at a feeding rate of 0.5 kg h^{-1} and a temperature of 220 °C

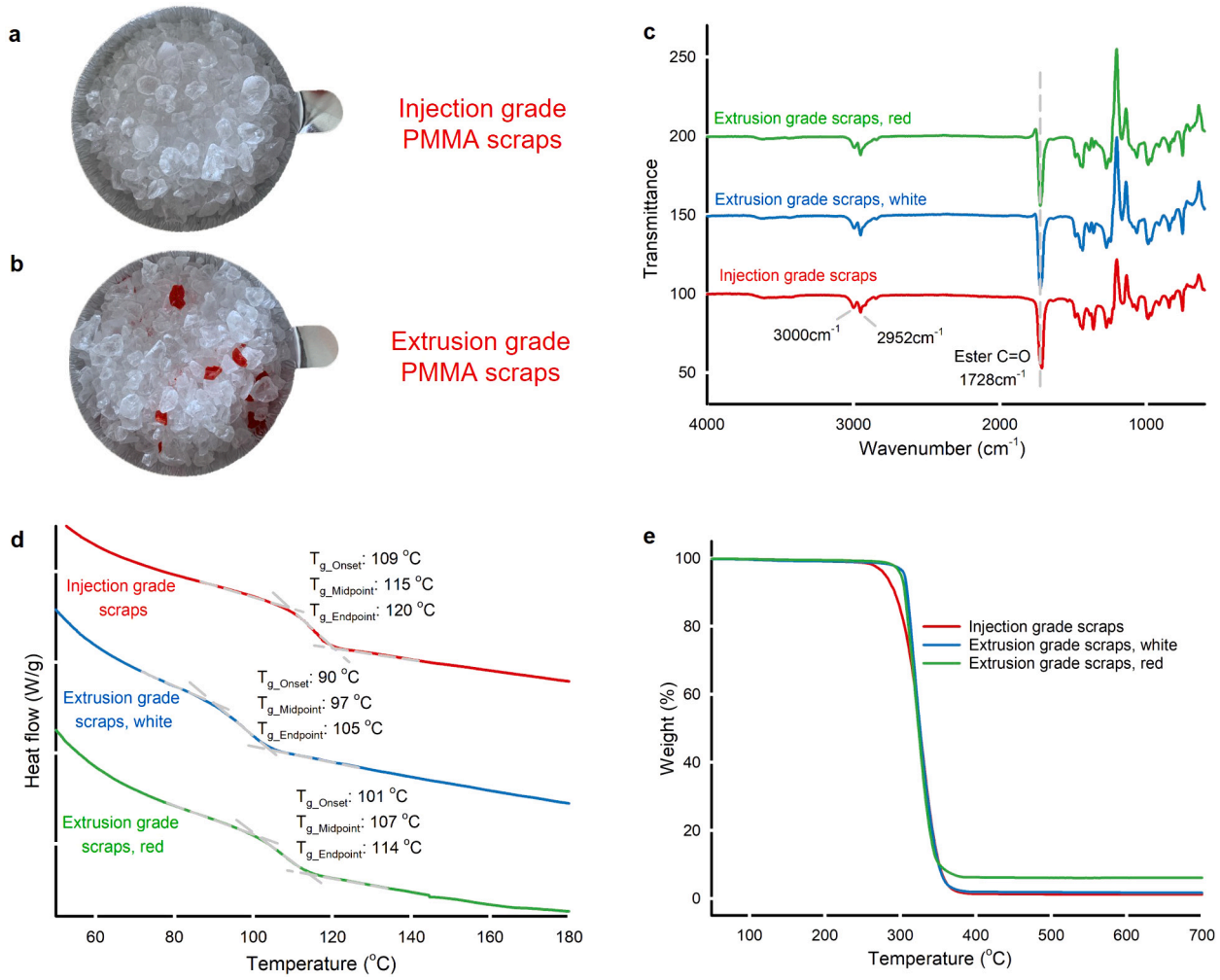

Fig. 3. Properties of injection-grade and extrusion-grade PMMA scraps. Injection-grade scraps consist of only one type of PMMA, while extrusion-grade scraps predominantly contain white PMMA with a small amount of red PMMA. **a**, Physical image of injection-grade PMMA scraps. **b**, Physical image of extrusion-grade PMMA scraps. **c**, FTIR spectra of injection-grade and extrusion-grade scraps from 4000 to 600 cm^{-1}. **d**, DSC curves of injection-grade and extrusion-grade scraps were recorded from 40 °C to 180 °C at a heating rate of 10 °C min^{-1} under a nitrogen atmosphere with a flow rate of 50 mL min^{-1}. **e**, Thermogravimetric curves of injection-grade and extrusion-grade scraps under N_2 atmosphere (60 mL min^{-1}) with a heating ramp of 5 °C min^{-1}.

shifted the RTD curves to shorter times, indicating a decreased mean residence time $\bar{t}$ (Fig. 2a). Additionally, this increase in screw speed reduced the N_{Pe} value from 17.6 to 16.6, demonstrating that higher screw speeds enhance axial mixing.

At a screw speed of 240 rpm and a temperature of 220 °C, increasing the feeding rate from 0.5 kg h^{-1} to 0.75 kg h^{-1} shifted the RTD curves to the left and reduced $\bar{t}$ to 9.4 min, but increased the N_{Pe} (Fig. 2b). The higher feeding rate resulted in a greater degree of fill, which weakens axial mixing [36,38].

Reducing the extrusion temperature from 220 °C to 200 °C at a screw speed of 240 rpm and a feeding rate of 0.5 kg h^{-1} decreased the N_{Pe} from 17.6 to 12, while slightly increasing the mean residence time, $\bar{t}$, from 11.7 min to 12.8 min (Fig. 2c). At higher processing temperatures, the viscosity and density of the melt decrease, enhancing the melt velocity (u). However, elevated temperatures also accelerate the thermal motion of molecules, leading to an increase in the axial dispersion coefficient (D). To prevent thermal degradation of PMMA during the RTD tests, we avoided higher extrusion temperatures. Within the temperature range of 200 °C to 220 °C, the increase in the axial dispersion coefficient (D) had a more pronounced effect on N_{Pe} than the corresponding increase in melt velocity (u).

Reactive extrusion hydrolysis involves a melt-solid-gas heterogeneous state, where effective mixing of catalysts with the melt and steam is crucial. While reduced axial mixing (higher N_{Pe}) decreases the formation of impurities, plug flow-like extrusion also reduces the axial mixing of catalysts within the PMMA melt. This degrades contact between catalysts and MMA, reducing MAA yield. Conversely, longer residence times enhance PMMA depolymerization by increasing PMMA conversion. However, extending the residence time decreases the overall productivity of the reactive extrusion hydrolysis process. Therefore, optimizing the axial mixing extent (N_{Pe}) and residence time is essential to achieve high PMMA conversion and yield of MMA and/or MAA while minimizing impurity levels.

3.2. Design of experiments (DOE)

To identify the key factors affecting reactive extrusion degradation, we employed a Plackett-Burman design of experiments. PMMA conversion (X_{PMMA}), yield (Y_i), selectivity (S_i), and recovered carbon (carbon balance) responded to five selected factors (Table 3). The Pareto charts revealed that no factors significantly affected X_{PMMA}, Y_{MMA}, Y_{MAA}, S_{MMA}, S_{MeOH}, or recovered carbon (Supplementary Fig. A.3a-c, e, g-h). However, temperature and catalyst type significantly affected Y_{MeOH} and S_{MAA} (Supplementary Fig. A.3d & f), which correspond to the MMA hydrolysis reaction. Vacuum degassing resulted in an irreversible loss of volatile vapors.

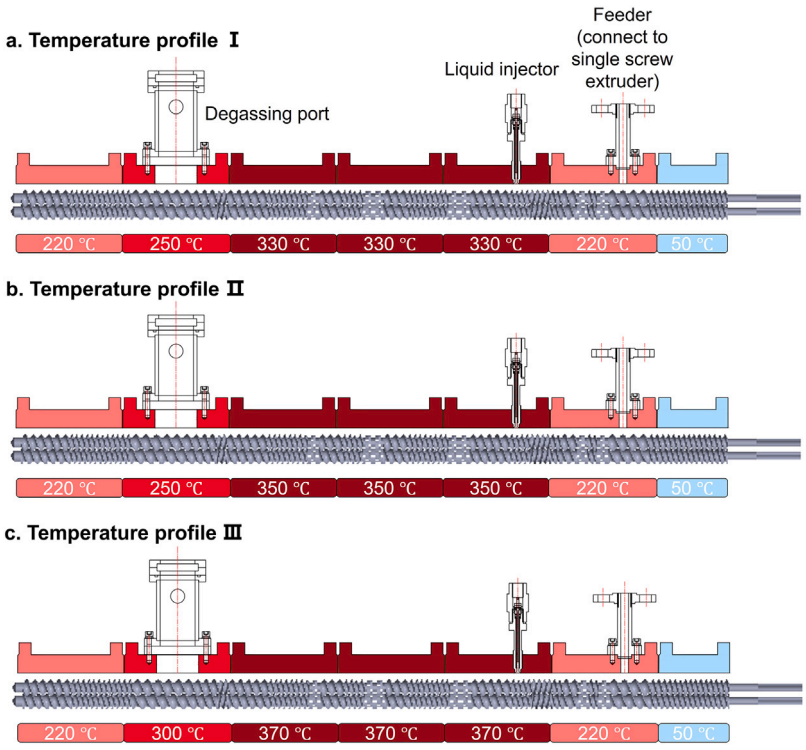

Fig. 4. Temperature profiles of PMMA reactive extrusion hydrolysis along the twin-screw extruder. The first barrel is set at 50 °C to protect the gearbox from overheating during direct melt injection. The second barrel is set at 220 °C to ensure successful melt injection while minimizing melt degradation. The final barrel is also set at 220 °C to cool the melt and terminate the degradation reaction. **a**, Temperature profile I features a maximum degradative extrusion temperature of 330 °C and a degassing temperature of 250 °C. **b**, Temperature profile II features a maximum degradative extrusion temperature of 350 °C and a degassing temperature of 250 °C. **c**, Temperature profile III features a maximum degradative extrusion temperature of 370 °C and a degassing temperature of 300 °C.

Table 3
Design of experiments (DOE) and results of DOE.

Run	Scrap	Cat.	$Q_{cat.}$ g h^{-1}	Q_{H_2O} mL min^{-1}	Degassing	T °C	Q^a_{PMMA} g h^{-1}	N_{TSE} rpm	X_{PMMA} %	Y_{MMA} %	Y_{MAA} %	Y_{MeOH} %	S_{MMA} %	S_{MAA} %	S_{MeOH} %	Recovered C^b mol %
1	Injection	Al_2O_3	13.6	2.7	Vacuum	350	740	240	33	6.3	0.7	0.2	19.1	2.2	0.5	74.3
2	Injection	Al_2O_3	8.9	1.8	Vacuum	330	488	240	24	3.1	0.2	0.1	13.1	0.9	0.4	79.7
3	Extrusion	Al_2O_3	9.0	1.8	Vacuum	350	491	360	43	5.0	1.0	0.2	11.4	2.3	0.5	62.9
4	Extrusion	HY(80)	9.0	1.8	Vacuum	350	493	360	19	6.8	1.1	0.5	35.9	5.6	2.4	89.5
5	Extrusion	HY(80)	14.2	2.7	Vacuum	330	775	240	4	0.9	0.5	0.2	23.3	11.9	5.9	97.8
6	Injection	HY(80)	13.6	2.7	Vacuum	350	740	360	31	13.8	0.9	0.3	44.3	2.8	1.1	83.9
7	Injection	Al_2O_3	8.9	1.8	Vacuum	330	488	360	24	3.5	0.2	0.1	14.4	0.9	0.4	79.6
8	Extrusion	HY(80)	9.0	1.8	Vacuum	330	493	240	3	1.6	0.4	0.3	55.8	15.0	9.2	99.4
9	Injection	HY(80)	13.6	2.7	Vacuum	330	740	360	4	2.6	0.6	0.2	59.6	14.0	5.3	99.1
10	Extrusion	Al_2O_3	13.4	2.7	Vacuum	350	733	240	25	4.3	0.7	0.2	16.9	2.8	0.7	79.9
11	Extrusion	Al_2O_3	13.4	2.7	Vacuum	330	733	360	10	1.0	0.1	0.1	9.7	0.7	0.5	90.7
12	Injection	HY(80)	9.0	1.8	Vacuum	350	491	240	51	20.4	1.2	0.5	40.3	2.4	0.9	71.5

Note: T-temperature, cat.-catalyst, $Q_{cat.}$-feeding rate of catalyst, Q_{H_2O}-liquid H_2O injection rate, Q_{PMMA}-PMMA scrap feeding rate, N_{TSE}-screw rotation speed of twin-screw extruder. a-PMMA feeding by a single screw extruder, b-considering carbon in residues and quantitatively analyzed liquid components MMA, MAA, methanol and a trace of acetone. Yield and selectivity to acetone were excluded in this table due to low concentration.

The X_{PMMA} of both extrusion- and injection-grade scraps increased as the temperature rose from 330 °C to 350 °C. A lower PMMA feeding rate, resulting in longer residence times, leads to increased PMMA conversion. Increasing the feeding rate shortens the residence time of the PMMA melt within the extruder and reduces axial mixing [39]. Although screw speed (N_{TSE}) did not significantly affect X_{PMMA} and MMA hydrolysis, increasing N_{TSE} decreased the residence time of the melt but enhanced axial mixing [40].

PMMA hydrolysis is a tandem reaction process. First, PMMA thermally depolymerizes to MMA, followed by the catalytic hydrolysis of MMA to MAA [12,19]. At higher reaction temperatures, the kinetics of PMMA depolymerization are faster than those of MMA hydrolysis, resulting in a much higher yield of MMA compared to MAA. The generation rate of MMA is primarily determined by barrel temperature and the mean residence time in the reaction zones of the twin-screw extruder, although mechanical shear also slightly contributes to PMMA degradation [41].

Selectivity to MAA was higher over HY(80) compared to Al_2O_3. The weight ratio of catalysts in the PMMA feed is set at 1.8%. This low catalyst/PMMA ratio may not achieve a high MAA yield due to insufficient contact between PMMA or MMA and the catalysts.

3.3. Properties of PMMA scraps

Injection-grade scraps contain only one type of PMMA, while extrusion- grade scraps include both white and red components (Fig. 3a & b). FTIR analysis exhibited a prominent peak at 1728 cm^{-1}, corresponding to the C=O stretch vibration. Additionally, two adjacent peaks were observed at 2952 cm^{-1} and 3000 cm^{-1}, attributed to the C-H stretching vibrations of $-CH_2$ and $-CH_3$, respectively [42–44] (Fig.

Table 4
Reactive extrusion hydrolysis of PMMA to MMA and MAA.

Run	Scrap	Cat.	Q^a_{Liquid} mL min^{-1}	Degassing	T °C	Q_{PMMA} g h^{-1}	N_{TSE} rpm	X_{PMMA} %	Y_{MMA} %	Y_{MAA} %	Y_{MeOH} %	S_{MMA} %	S_{MAA} %	S_{MeOH} %	Recovered C^b mol %
N1	Injection	0.01 g mL^{-1} PTA	3.6	Vacuum	350	500	240	62	22	1.2	1.1	36	2.0	1.8	62
N2	Injection	0.01 g mL^{-1} PTA	3.6	Vacuum	330	500	240	12	2	0.3	0.4	13	2.4	3.0	90
N3	Injection	10% HY(80)	3.6	Vacuum	350	450	240	59	7	2.0	0.9	11	3.4	1.5	50
N4	Injection	10% HY(80)	3.6	Atmosphere	370	444	240	100	67	5.3	2.0	65	5.2	1.9	71
N5	Injection	10% HY(80)	3.6	Atmosphere	350	444	240	52	32	4.9	1.0	62	9.4	1.8	86
N6	Injection	10% HY(80)+0.01 g mL^{-1} PTA	3.6	Atmosphere	370	444	240	98	57	5.5	2.0	58	5.7	2.0	66
N7	Injection	0.05 g mL^{-1} KOH	3.6	Atmosphere	370	500	240	86	27	0.8	7.9	31	0.9	9.2	49
N8	Injection	0.05 mol L^{-1} H_2SO_4	3.6	Atmosphere	370	458	240	65	51	0.6	14.0	77	0.9	21.4	100
N9	Injection	None (H_2O only)	3.6	Vacuum	350	500	240	31	8	1.0	0.2	25	3.2	0.6	78
N10	Injection	None (H_2O only)	3.6	Atmosphere	370	500	240	96	89	0.0	0.1	92	0.0	0.1	92
N11	Injection	None	0.0	Atmosphere	370	500	240	82	75	0.0	0.0	91	0.0	0.0	93

Note: a-Q_{Liquid}-H_2O or solutions injection rate, b-considering carbon in extrudates and quantitatively analyzed liquid components MMA, MAA, methanol and a trace of acetone.

3c). These characteristic peaks confirm that all scraps are composed of only PMMA.

The midpoint glass transition temperature (T_g) of injection-grade scraps (T_g = 109 °C) is higher than that of the white (T_g = 90 °C) and red (T_g = 101 °C) components in extrusion-grade scraps (Fig. 3d). The T_g of all scraps ranges from 55 °C to 130 °C, indicating an atactic tacticity [45]. Higher T_g values are closer to syndiotactic tacticity, while lower T_g values are closer to isotactic tacticity [46]. The lack of a melting point in the DSC curves indicates that the used PMMA is amorphous and further confirms that it is atactic [47].

Thermogravimetric analysis revealed that injection-grade scraps began to degrade at a lower temperature of 250 °C compared to the white and red components in extrusion-grade scraps in N_2 (Fig. 3e). The white and red components in extrusion-grade scraps exhibited similar thermal degradation behavior, starting to lose weight at 280 °C. Injection-grade scraps and white extrusion-grade scraps left residues of approximately 1% to 2%, while red extrusion-grade scraps had 6% non-thermally degradable residues. These residues are due to fillers or additives in the scraps.

3.4. Optimization of extrusion reaction conditions

To increase the reaction time of PMMA depolymerization and MMA hydrolysis within the twin-screw extruder, we found that a lower screw speed and feeding rate are preferred. Following DOE experiments, we tested higher reaction temperatures and higher weight ratios of HY(80) to PMMA feed. Under optimized conditions, we fed 0.5 kg h^{-1} of PMMA scraps or mixtures of PMMA scraps and solid catalysts at a screw speed of 240 rpm. Injection-grade scraps depolymerize at lower temperatures compared to extrusion-grade scraps. Based on the DOE tests, we focused on recycling injection-grade scraps. To achieve higher PMMA conversion (X_{PMMA}), we increased the temperature of the reaction zones from 330 °C/350 °C to 370 °C and the degassing temperature from 250 °C to 300 °C (Fig. 4).

To compare the hydrolysis effects of solid and liquid catalysts, we used solid HY(80) catalyst and liquid catalysts including PTA, KOH, and H_2SO_4. To increase the contact between solid HY(80) and the PMMA melt, we increased the weight ratio of HY(80) to PMMA feed from 1.8% (as used in DOE) to 10%. Within the reaction zones, the components in the extruder exist in a melt-solid-gas heterogeneous state. Increasing the steam fraction in this heterogeneous system may contribute to higher PMMA depolymerization and MMA hydrolysis rates. In this work, at a feeding rate of 0.5 kg h^{-1}, we increased the water injection rate from 1.8 mL min^{-1} to 3.6 mL min^{-1}.

3.4.1. Impact of catalysts on hydrolysis and extrusion processes

Compared to hydrolysis extrusion with HY(80), PTA, KOH, and H_2SO_4, non-catalytic hydrolysis extrusion (N10) without catalysts at 370 °C and with 3.6 mL min^{-1} water injection exhibited the highest yield of MMA (Y_{MMA} = 89%) (Fig. 5a & Table 4). At 370 °C, pyrolysis extrusion (N11) without steam and catalysts achieved the second highest MMA yield (Y_{MMA} = 75%), though the PMMA conversion was lower at 82% compared to the PMMA conversion (X_{PMMA} = 96%) in non-catalytic hydrolysis extrusion. This confirms that steam accelerates PMMA thermal depolymerization.

Hydrolysis extrusion with 10% HY(80) at 370 °C (N4) resulted in a near-complete PMMA conversion (X_{PMMA} = 100%). Under the combined presence of 10% HY(80) and PTA solution (N6), hydrolysis extrusion at 370 °C showed a PMMA conversion of 98% but a lower MMA yield (Y_{MMA} = 57%) compared to hydrolysis extrusion with 10% HY(80) (N4) alone (Y_{MMA} = 67%). The co-injection of PTA solution and solid HY(80) (N6) slightly increased the MAA yield from 5.3% to 5.5% compared to hydrolysis extrusion with 10% HY(80).

Between co-injection of PTA and HY(80) (N6) and single injection of HY(80) (N4), the yields of MAA and methanol were similar, but the presence of PTA reduced the MMA yield by 15%, indicating that PTA catalyzed the conversion of PMMA or MMA to other by-products. At a hydrolysis extrusion temperature of 370 °C, the injection of KOH (N7) and H_2SO_4 (N8) exhibited PMMA conversions of 86% and 65%, respectively. Hydrolysis extrusion with KOH (N7) resulted in the lowest MMA yield (Y_{MMA} = 27%) and a methanol yield of 7.9%. Hydrolysis extrusion with H_2SO_4 (N8) produced a MAA yield of 0.6% and the highest methanol yield (Y_{MeOH} = 14%) among all tests.

Both strong acids and strong alkalis are common ester hydrolysis catalysts. H_2SO_4 directly converts PMMA into PMAA or poly(MMA-co-MAA) copolymer and methanol by hydrolyzing ester groups on the PMMA chain [48,49]. In contrast, KOH solution reacts with ester groups on PMMA to form PMAA potassium salt or poly(MMA-co-MAA) potassium salt and methanol [49,50]. Hydrolysis extrusion with H_2SO_4 (N8) or KOH (N7) solution produced a significantly higher yield of methanol compared to MAA (Table 4), confirming that direct hydrolysis of PMMA generates additional methanol.

3.4.2. Impact of temperature on hydrolysis and extrusion processes

At a screw speed of 240 rpm and under atmospheric degassing, increasing the reaction temperature from 350 °C (N5) to 370 °C (N4) increased PMMA conversion from 52% to 100% (Fig. 5b & Table 4). At 370 °C (N4), injection-grade scraps were almost completely degraded. The selectivity to MMA increased from 62% at 350 °C to 65% at 370 °C, indicating that the temperature rise had a minimal effect on S_{MMA}. The selectivity to methanol remained nearly unchanged, while the selectivity to MAA was almost halved, dropping from 9.4% at 350 °C to 5.2% at 370 °C. This suggests that a lower reaction temperature (i.e., 350 °C) favors MMA hydrolysis, despite higher temperatures (i.e., 370 °C) accelerating PMMA depolymerization. At higher temperatures, the rate of PMMA depolymerization exceeds that of MMA hydrolysis, indicating that the depolymerization reaction has a higher activation energy than MMA hydrolysis [51]. We attribute the observed difference in S_{MAA} to the over-cracking of MAA at 370 °C.

3.4.3. Impact of degassing method on hydrolysis and extrusion processes

Degassing method determines the carbon balance of hydrolysis extrusion. At a screw speed of 240 rpm and a reaction temperature of 350 °C, hydrolysis extrusion with 10% HY(80) under vacuum degassing (N3) yielded only 6.7% MMA (Fig. 5c & Table 4). The PMMA conversion was 59%, but the recovered carbon percentage was merely 50%, indicating significant weight loss due to vacuum degassing. In contrast, atmospheric degassing (N5) resulted in a PMMA conversion of 52% and a substantially higher recovered carbon percentage of 86%.

Vacuum degassing enhanced the devolatilization of gaseous components from the extruder. However, it also created mists, complicating the condenser's ability to condense these gaseous components [52]. Consequently, product losses during vacuum degassing were attributed to the vacuum pump discharge. Atmospheric degassing, on the other hand, proved more effective for product collection. Steam acted as a stripping agent, facilitating devolatilization, thereby allowing atmospheric conditions to effectively cool the condensable gaseous components [53].

3.5. Solid residues analysis

Hydrolysis extrusion at 330 °C and 350 °C resulted in a high amount of residues containing unreacted PMMA, catalysts and by-products (≥38%) (Table 4). FTIR confirmed that non-catalytic hydrolysis at 350 °C without catalysts (N9) and hydrolysis extrusion with 10% HY(80) (N3) produced only PMMA residues with catalysts, indicating PMMA depolymerization followed by MMA hydrolysis (Fig. 6a & Fig. 7). Hydrolysis extrusion with PTA solution at 330 °C (N2) also left PMMA residues. However, residues obtained after hydrolysis extrusion with PTA solution at 350 °C exhibited two twin peaks at 1762 cm^{-1} and 1806 cm^{-1}, attributed to the acid anhydride group [54]. Specifically, the double peaks at 1762 cm^{-1} and 1806 cm^{-1} correspond to the structure of intramolecular six-member glutaric anhydride formed between two adjacent carboxyl groups [48,55]. During hydrolysis extrusion, in addition to MMA hydrolysis, PTA also hydrolyzed partial esters groups on PMMA directly to form acid groups. Subsequently, two adjacent carboxyl groups dehydrated to form six-member glutaric anhydride on the PMMA chain (Fig. 7). PMMA hydrolysis to PMAA can also be catalyzed by strong acids, such as sulfuric acid [48].

Thermogravimetric analysis (TGA) revealed two major mass loss stages between 230 °C and 380 °C, and between 380 °C and 500 °C in the residues obtained from PMMA hydrolysis extrusion with PTA at 350 °C (N1). In contrast, residues from PMMA extrusion with PTA at 330 °C (N2) exhibited a single mass loss stage between 250 °C and 400 °C (Fig. 6b).

The single mass loss stage in N2 residues (250 °C to 400 °C) and the first-stage mass loss in N1 residues (230 °C to 380 °C) were attributed to PMMA thermal depolymerization. However, the second-stage mass loss (380 °C to 500 °C) in N1 residues was attributed to the thermal degradation of acid anhydride. During thermal degradation of PMAA, PMAA dehydrates at around 220 °C to form acid anhydride, which exhibits a maximum degradation rate at approximately 410 °C [55]. This result further confirmed the formation of poly(MMA-co-MAA) copolymer during hydrolysis extrusion with PTA solutions and the presence of acid anhydride groups on the extrudates.

The residues obtained from hydrolysis extrusion with 10% HY(80) at 350 °C (N3) displayed a shifted weight loss curve, starting from 250 °C and ending at 400 °C, indicating that HY(80) increases the PMMA degradation temperature (Fig. 6b). A slight weight loss after 396 °C was attributed to the continuous reversible dehydration of the HY(80) framework [56] and the dehydration of coke formed in HY(80) during hydrolysis extrusion.

Morphological analysis revealed a dense surface on residues obtained from PMMA hydrolysis extrusion with PTA at 350 °C (N1) (Fig. 6c) and a porous surface on residues obtained from PMMA hydrolysis extrusion with 10% HY(80) (N3) (Fig. 6d). Both N1 and N3 residues were extruded under vacuum degassing conditions. The liquid PTA solutions did not induce significant pores or cracks. However, the solid HY(80) powder adhered to the PMMA surface, resulting in an uneven

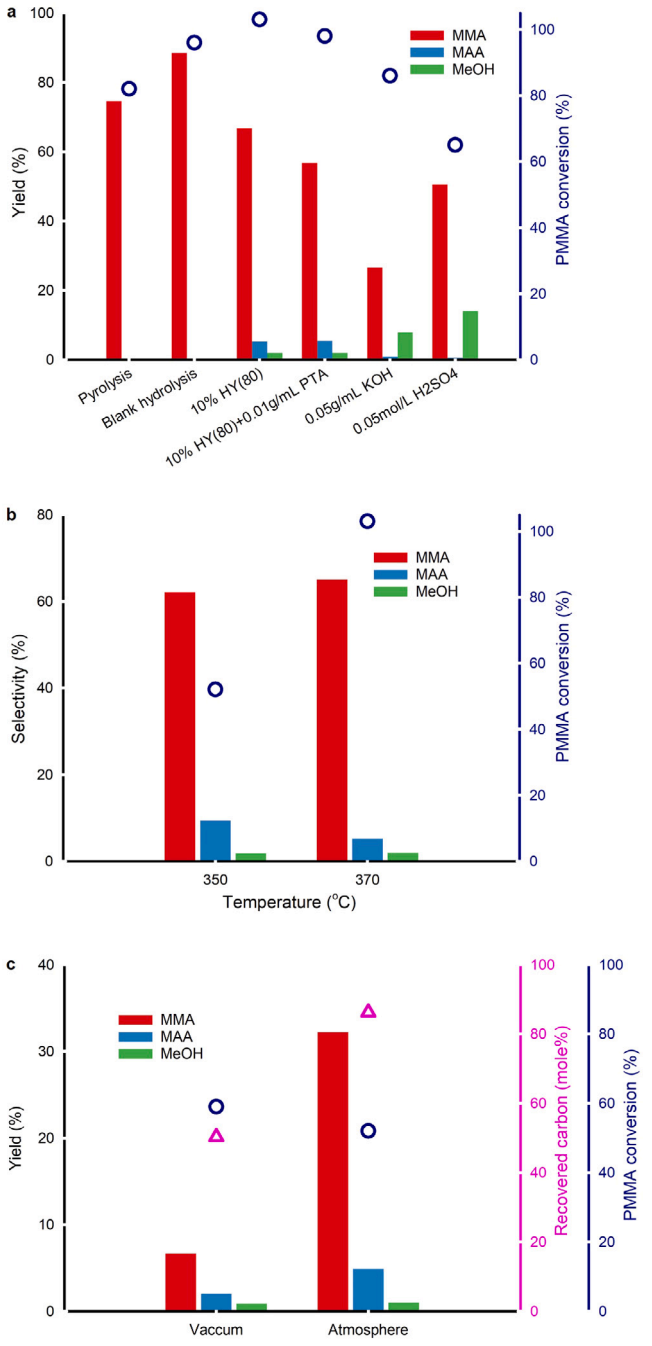

Fig. 5. PMMA reactive extrusion hydrolysis with and without catalysts. The optimized twin-screw rotation speed is 240 rpm, with a scrap feeding rate of 0.5 $kg\,h^{-1}$. **a**, Yields of MMA, MAA, and MeOH (left axis, bar), and PMMA conversion (right axis, hollow circle) with and without catalysts at 370 °C for a one-hour reaction, with a liquid injection rate of 3.6 $mL\,min^{-1}$ and under atmospheric degassing, excluding pyrolysis. **b**, The effect of hydrolysis temperature on the selectivity to MMA, MAA, and MeOH (left axis, bar), and PMMA conversion (right axis, hollow circle) for a one-hour reaction with 10% HY(80) feeding and a liquid injection rate of 3.6 $mL\,min^{-1}$ under atmospheric degassing. **c**, The effect of degassing methods on the yields of MMA, MAA, and MeOH (left axis, bar), and the recovered carbon (right axis, pink hollow triangle), as well as PMMA conversion (right axis, dark blue hollow circle) for a one-hour reaction at 350 °C with 10% HY(80) feeding and a liquid injection rate of 3.6 $mL\,min^{-1}$. (For interpretation of the references to color in this figure legend, the reader is referred to the web version of this article.)

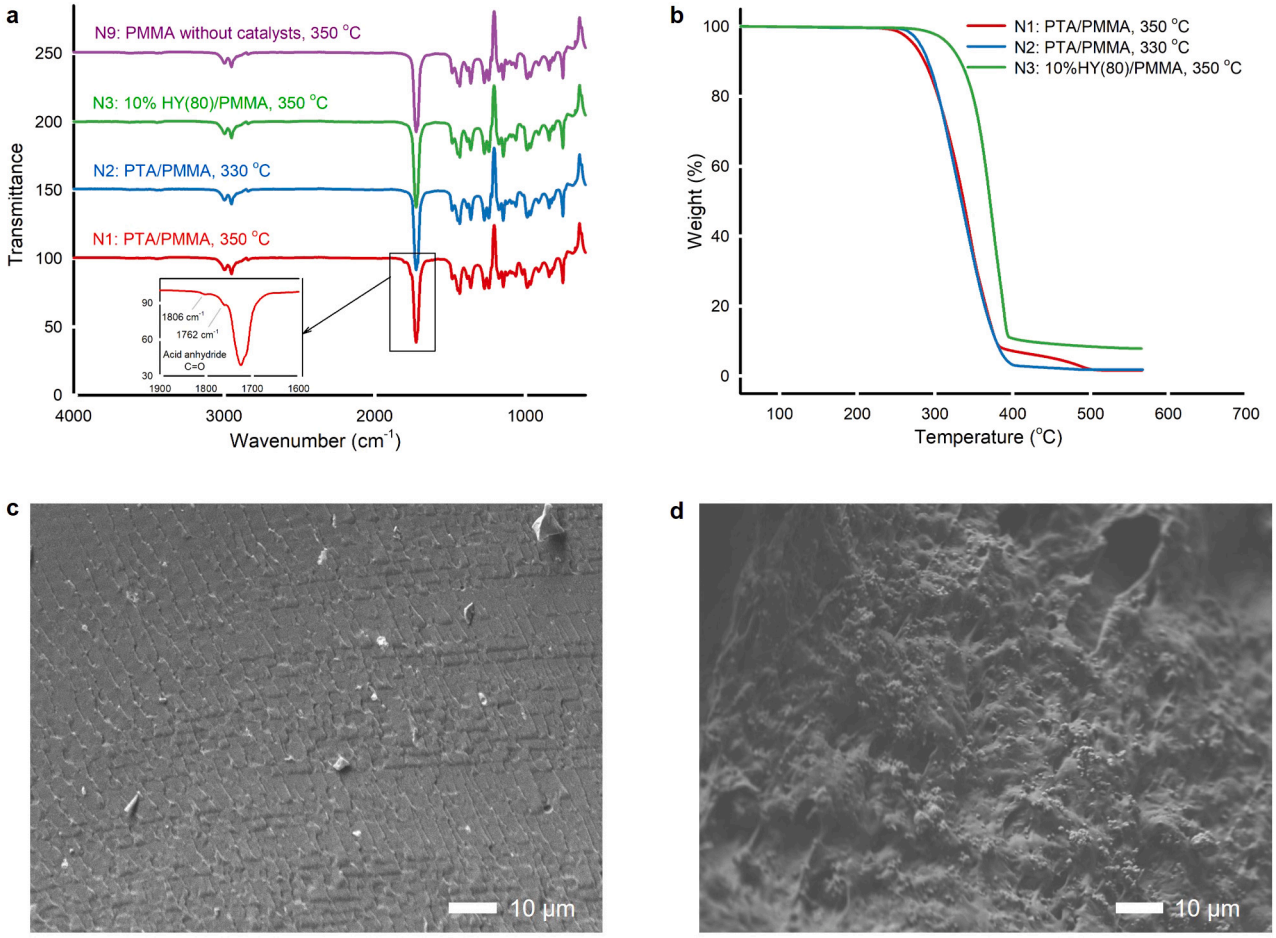

Fig. 6. Analysis of solid residue after PMMA reactive extrusion hydrolysis. All reactions were conducted for one hour with a twin-screw rotation speed of 240 rpm and a liquid injection rate of 3.6 mL min^{-1}. **a**, FTIR spectra of the extrudates from 4000 to 600 cm^{-1}. **b**, Thermogravimetric curves of the extrudates under N_2 atmosphere (60 mL min^{-1}) with a heating ramp of 5 °C min^{-1}. **c**, SEM images of PTA/PMMA (N1) extrudates. **d**, SEM images of 10% HY(80)/PMMA (N3) extrudates.

texture. The large pores and cracks were attributed to bubble collapse during the process. The hydrolysis extrusion functioned similarly to a forming process.

3.6. Mechanism of hydrolysis extrusion

Without steam, PMMA thermally depolymerizes into MMA monomer via a free radical mechanism [9,10]. We propose a PMMA hydrolysis extrusion mechanism over solid HY(80) and liquid PTA and sulfuric acid solutions based on experimental data (Fig. 7). PMMA thermal depolymerization without catalysts dominated during the hydrolysis extrusion. Random chain scission above 330 °C produced tertiary alkyl radicals, which subsequently underwent unzipping to generate MMA monomer [15]. Some MMA monomers were hydrolyzed into MAA and methanol over HY(80) or acid catalysts in the reaction zones (≥330 °C). Most MMA did not contact the catalyst during extrusion, resulting in high MMA yield and low MAA yield. A small amount of primary alkyl radicals was generated during random chain scission, followed by the formation of $CH_3O(CO)\cdot$ free radical fragments [10]. $CH_3O(CO)\cdot$ free radical fragments combined with a proton to generate methanol and CO [27]. This mechanism generates additional methanol beyond what is produced by the hydrolysis of PMMA and MMA.

With HY(80) and liquid acid solutions, some PMMA chains were hydrolyzed to poly(MMA-co-MAA) copolymer and methanol, followed by the dehydration of two adjacent acid groups to form six-member glutaric anhydride. Glutaric anhydride may undergo further decomposition, resulting in the formation of a hydrocarbon backbone and gaseous byproducts. Diluted sulfuric acid (0.05 mol L^{-1}) hydrolyzed PMMA into poly(MMA-co-MAA) copolymer and/or PMAA more effectively than PTA solutions (0.01 g mL^{-1}) and HY(80) at 370 °C. Acetone, which results from the over-cracking of MMA and MAA during PMMA pyrolysis or hydrolysis [12], was insignificant in the hydrolysis extrusion due to low concentration. We did not investigate gaseous products as our focus was primarily on the non-gaseous components.

Hydrolysis extrusion with a strong alkaline (KOH) solution produced methanol by directly hydrolyzing PMMA to poly(MMA-co-MAA) and/or PMAA potassium salt, along with partial MMA hydrolysis to MAA. Concurrently, PMMA depolymerization and direct hydrolysis to poly(MMA-co-MAA) and/or PMAA potassium salt occurred.

4. Conclusion

Reactive extrusion offers a continuous method for recycling PMMA scraps, producing MMA and/or MAA. In this process, gaseous products are collected from the degassing barrel via vacuum or atmospheric devolatilization, while solid residues are extruded from the die. The continuous operation feature of reactive extrusion makes it an ideal alternative to traditional PMMA recycling reactors, such as stirred tanks, molten metal reactors, and fluidized beds. In this study, we developed a pilot-scale two-stage reactive extrusion system to recycle injection- and extrusion-grade PMMA scraps at 330 °C to 370 °C. A first-stage single screw extruder, acting as a melt feeder, injected PMMA melt with/without solid catalysts into a second-stage twin-screw reactive extruder. The direct feeding of melt into the twin-screw extruder,

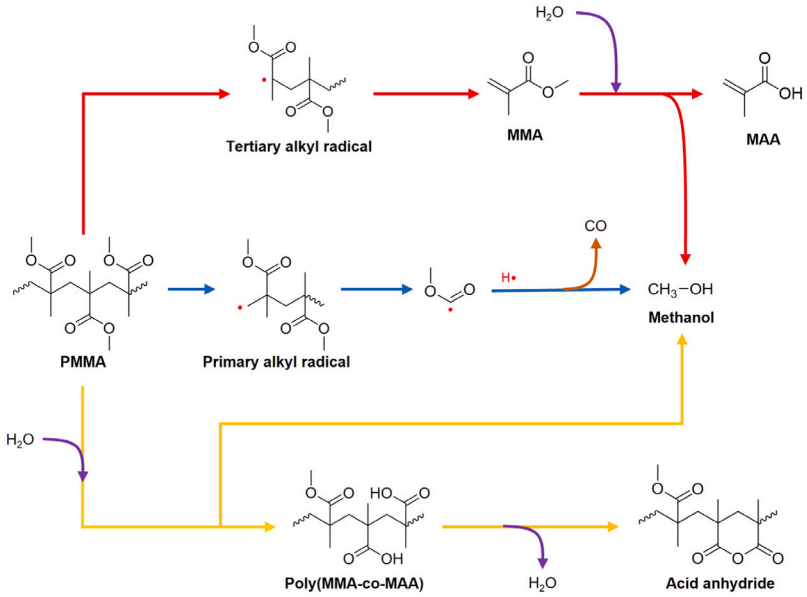

Fig. 7. Mechanism of PMMA hydrolysis extrusion with solid HY(80) and liquid acid solutions.

combined with the designed screw configuration, created a dynamic sealing zone prior to the liquid injection and reaction zones.

RTD tests conducted prior to all REX tests showed that lower screw speed and feeding rate increased melt mean residence time, ensuring sufficient reaction time within the extruder. However, extended residence times would lead to reduced productivity and negatively impact the economics of reactive extrusion recycling of PMMA. A Plackett-Burman design identified catalyst type and temperature as significant factors for MMA hydrolysis within the reactive extruder. Based on DOE results, we optimized the reaction temperature profile along the second-stage twin-screw extruder, achieving the highest reaction temperature of 370 °C and the highest degassing temperature of 300 °C. Along with the optimized reaction temperature profile, increasing the water injection rate to 3.6 mL min^{-1} and switching from vacuum to atmospheric degassing yielded the highest MMA yield (Y_{MMA} = 89%) and 96% PMMA conversion without any catalysts. Under optimized conditions, increasing the weight ratio of HY(80) to PMMA to 10% resulted in a 5.3% yield to MAA and a 67% yield to MMA, as well as near-complete PMMA conversion. The synergies of solid HY(80) and PTA solutions achieved the highest yield to MAA (Y_{MAA} = 5.5%) and 98% PMMA conversion. The low yield to MAA was attributed to a much faster PMMA depolymerization rate compared to MMA hydrolysis and an insufficient amount of hydrolysis catalysts. Solid residue analysis revealed that direct hydrolysis of PMMA to poly(MMA-co-MAA) occurred with PTA catalysts. Extrusion hydrolysis with diluted H_2SO_4 solution (0.05 mol L^{-1}) achieved the highest yield to methanol (Y_{MeOH} = 14%), indicating that the diluted strong acid solution directly hydrolyzed PMMA to PMAA or poly(MMA-co-MAA) copolymer, with PMMA depolymerization (Y_{MMA} = 51%). The obtained PMAA or poly(MMA-co-MAA) copolymer tends to form six-member glutaric anhydride via further dehydration. A strong alkaline (KOH) solution directly hydrolyzed PMMA to produce poly(MMA-co-MAA) and/or PMAA potassium salt and methanol.

CRediT authorship contribution statement

Yanfa Zhuang: Writing – review & editing, Writing – original draft, Visualization, Validation, Methodology, Investigation, Formal analysis, Data curation, Conceptualization. **Tien Dat Nguyen:** Writing – review & editing, Visualization, Methodology, Investigation, Formal analysis, Data curation. **Mahdi Sharifian:** Writing – review & editing, Investigation. **Jean-Luc Dubois:** Writing – review & editing, Supervision. **Abdellah Ajji:** Writing – review & editing, Supervision, Resources. **Gregory Patience:** Writing – review & editing, Supervision, Resources, Project administration, Funding acquisition.

Declaration of competing interest

The authors declare the following financial interests/personal relationships which may be considered as potential competing interests: Gregory S. Patience reports financial support was provided by Natural Sciences and Engineering Research Council of Canada. Gregory S. Patience reports financial support was provided by Arkema. Gregory S. Patience reports financial support was provided by Lavergne. If there are other authors, they declare that they have no known competing financial interests or personal relationships that could have appeared to influence the work reported in this paper.

Acknowledgments

The authors thank Polymer Montreal for providing extrusion- and injection-grade PMMA scraps; and Prof. Davide Brambilla and Shihao Pei at Université de Montréal for fluorescence testing. This work was supported by the Natural Sciences and Engineering Research Council of Canada (ALLRP-573784-22 CRSNG) and Arkema & Lavergne (CDT 051087).

Appendix A. Supplementary data

Supplementary material related to this article can be found online at https://doi.org/10.1016/j.cej.2025.162709.

Data availability

Data will be made available on request.

References

[1] E. Erickson, Shaping a federal strategy for chemical recycling: Moving toward sensible applications of emerging technologies in US plastic waste management, Environ. Prog. Sustain. Energy (2024) e14333.

[2] B.T. Nicholls, B.P. Fors, Closing the loop on thermoset plastic recycling, Science 384 (6692) (2024) 156–157.

[3] R.S. Lampitt, S. Fletcher, M. Cole, A. Kloker, S. Krause, F. O'Hara, P. Ryde, M. Saha, A. Voronkova, A. Whyle, Stakeholder alliances are essential to reduce the scourge of plastic pollution, Nat. Commun. 14 (1) (2023) 2849.

[4] B. Hu, S. Wang, J. Yan, H. Zhang, L. Qiu, W. Liu, Y. Guo, J. Shen, B. Chen, C. Shi, X. Ge, Review of waste plastics treatment and utilization: Efficient conversion and high value utilization, Process. Saf. Environ. Prot. (2024).

[5] U. Ali, K.J.B.A. Karim, N.A. Buang, A review of the properties and applications of poly (methyl methacrylate)(PMMA), Polym. Rev. 55 (4) (2015) 678–705.

[6] J. De Tommaso, J.-L. Dubois, Risk analysis on PMMA recycling economics, Polymers 13 (16) (2021) 2724.

[7] M. Sponchioni, S. Altinok, Poly (methyl methacrylate): Market trends and recycling, in: D. Moscatelli, M. Pelucchi (Eds.), in: Advances in Chemical Engineering, vol. 60, Elsevier, Cambridge, 2022, pp. 269–287.

[8] M. Newborough, D. Highgate, J. Matcham, Thermal depolymerisation of poly-methyl-methacrylate using mechanically fluidised beds, Appl. Therm. Eng. 23 (6) (2003) 721–731.

[9] E. Esmizadeh, S. Khalili, A. Vahidifar, G. Naderi, C. Dubois, Waste polymethyl methacrylate (PMMA): Recycling and high-yield monomer recovery, in: L. Martínez, O. Kharissova, B. Kharisov (Eds.), Handbook of Ecomaterials, Springer International Publishing, Cham, 2018, pp. 1–33.

[10] E.K. Moens, K. De Smit, Y.W. Marien, A.D. Trigilio, P.H. Van Steenberge, K.M. Van Geem, J.-L. Dubois, D.R. D'hooge, Progress in reaction mechanisms and reactor technologies for thermochemical recycling of poly (methyl methacrylate), Polymers 12 (8) (2020) 1667.

[11] J. Dubois, Guidelines for PMMA depolymerization at pilot and industrial scale, 2022, https://www.researchgate.net/. (Accessed April 2022).

[12] O.V. Chub, N. Saadatkhah, J.-L. Dubois, G.S. Patience, Fluidized bed poly (methyl methacrylate) thermolysis to methyl methacrylate followed by catalytic hydrolysis to methacrylic acid, Appl. Catal. A: Gen. 638 (2022) 118637.

[13] S. El-Bashir, N. Althumairi, N. Alzayed, Durability and mechanical performance of PMMA/stone sludge nanocomposites for acrylic solid surface applications, Polymers 9 (11) (2017) 604.

[14] K. Gkaliou, L. Benedini, Z. Sárossy, C.D. Jensen, U.B. Henriksen, A.E. Daugaard, Recycled PMMA prepared directly from crude MMA obtained from thermal depolymerization of mixed PMMA waste, Waste Manage. 164 (2023) 191–199.

[15] C.B. Godiya, S. Gabrielli, S. Materazzi, M.S. Pianesi, N. Stefanini, E. Marcantoni, Depolymerization of waste poly (methyl methacrylate) scraps and purification of depolymerized products, J. Environ. Manag. 231 (2019) 1012–1020.

[16] W. Kaminsky, J. Franck, Monomer recovery by pyrolysis of poly (methyl methacrylate)(PMMA), J. Anal. Appl. Pyrolysis 19 (1991) 311–318.

[17] B. Meek, J.W. Bridges, A. Fasey, U.G. Sauer, Evidential requirements for the regulatory hazard and risk assessment of respiratory sensitisers: methyl methacrylate as an example, Arch. Toxicol. 97 (4) (2023) 931–946.

[18] S. Kleinbeck, M. Schäper, M. Pacharra, M.L. Lehmann, K. Golka, M. Blaszkewicz, T. Brüning, C. van Thriel, A short-term inhalation study to assess the reversibility of sensory irritation in human volunteers, Arch. Toxicol. 94 (2020) 1687–1701.

[19] O.V. Chub, J.-L. Dubois, G.S. Patience, Tandem fluidized bed/milli-second fixed bed reactor produces methacrylic acid from poly (methyl methacrylate), Appl. Catal. A: Gen. 647 (2022) 118887.

[20] M. Pirmoradi, J.R. Kastner, Synthesis of methacrylic acid by catalytic decarboxylation and dehydration of carboxylic acids using a solid base and subcritical water, ACS Sustain. Chem. Eng. 5 (2) (2017) 1517–1527.

[21] G. Swift, Acrylic (and methacrylic) acid polymers, Encycl. Polym. Sci. Technol. 1 (2002).

[22] M.J.D. Mahboub, J.-L. Dubois, F. Cavani, M. Rostamizadeh, G.S. Patience, Catalysis for the synthesis of methacrylic acid and methyl methacrylate, Chem. Soc. Rev. 47 (20) (2018) 7703–7738.

[23] K. Nagai, T. Ui, Trends and future of monomer-MMA technologies, Sumitomo Chem 2 (2004) 4–13.

[24] Y. Wu, M. Shetty, K. Zhang, P.J. Dauenhauer, Sustainable hybrid route to renewable methacrylic acid via biomass-derived citramalate, ACS Eng. Au 2 (2) (2021) 92–102.

[25] J. Lebeau, J.P. Efromson, M.D. Lynch, A review of the biotechnological production of methacrylic acid, Front. Bioeng. Biotechnol. 8 (2020) 207.

[26] J.-L. Dubois, US2021/04028A1-Recovery of (meth) acrylic resin by depolymerization and hydrolysis, 2021.

[27] Y. Zhuang, N. Saadatkhah, T.-D. Nguyen, J. De Tommaso, C.Y.J. Ng, C. Wang, A. Ajji, G.S. Patience, Upcycling polymethyl methacrylate to methacrylic acid, React. Chem. Eng. (2025).

[28] J. De Tommaso, F. Galli, T.D. Nguyen, Y. Zhuang, J.-L. Dubois, G.S. Patience, Waste artificial marble pyrolysis and hydrolysis, Waste Manage. 195 (2025) 129–144.

[29] Y. Zhuang, N. Saadatkhah, M.S. Morgani, T. Xu, C. Martin, G.S. Patience, A. Ajji, Experimental methods in chemical engineering: Reactive extrusion, Can. J. Chem. Eng. 101 (1) (2023) 59–77.

[30] MMAtwo, MMAtwo in position to benchmark its results with state of the art virgin and regenerated MMA, 2022, https://www.mmatwo.eu. (Accessed March 2023).

[31] R.L. Plackett, J.P. Burman, The design of optimum multifactorial experiments, Biometrika 33 (4) (1946) 305–325.

[32] R. Bardestani, G.S. Patience, S. Kaliaguine, Experimental methods in chemical engineering: specific surface area and pore size distribution measurements—BET, BJH, and DFT, Can. J. Chem. Eng. 97 (11) (2019) 2781–2791.

[33] M. Sharifian, N. Hudon, E. Pahija, G.S. Patience, Feedback control strategy of Fischer-Tropsch process in a micro-GtL plant, Chem. Eng. Res. Des. (2024).

[34] A. Bérard, B. Blais, G.S. Patience, Residence time distribution in fluidized beds: diffusion, dispersion, and adsorption, Adv. Powder Technol. 32 (5) (2021) 1677–1687.

[35] O. Levenspiel, Chemical Reaction Engineering, John Wiley & Sons, New York, 1998.

[36] N. Frame, Operational characteristics of the co-rotating twin-screw extruder, Technol. Extrus. Cook. (1994) 1–51.

[37] E.N. Kimuli, I.I. Onyemelukwe, B. Benyahia, C.D. Rielly, Characterisation of axial dispersion in a Meso-scale Oscillatory Baffled Crystalliser using a Numerical Approach, in: A. Espuña, M. Graells, L. Puigjaner (Eds.), in: Computer Aided Chemical Engineering, vol. 40, Elsevier, Barcelona, 2017, pp. 223–228.

[38] P. Ainsworth, S. Ibanoglu, G.D. Hayes, Influence of process variables on residence time distribution and flow patterns of tarhana in a twin-screw extruder, J. Food Eng. 32 (1) (1997) 101–108.

[39] H. Fang, F. Mighri, A. Ajji, P. Cassagnau, S. Elkoun, Flow behavior in a corotating twin-screw extruder of pure polymers and blends: Characterization by fluorescence monitoring technique, J. Appl. Polym. Sci. 120 (4) (2011) 2304–2312.

[40] L. Kotamarthy, S. Karkala, A. Dan, A.D. Román-Ospino, R. Ramachandran, Investigating the effects of mixing dynamics on twin-screw granule quality attributes via the development of a physics-based process map, Pharmaceutics 16 (4) (2024) 456.

[41] C. Capone, L. Di Landro, F. Inzoli, M. Penco, L. Sartore, Thermal and mechanical degradation during polymer extrusion processing, Polym. Eng. Sci. 47 (11) (2007) 1813–1819.

[42] B.-S. Lee, Y.-J. Chen, T.-C. Wei, T.-L. Ma, C.-C. Chang, Comparison of antibacterial adhesion when salivary pellicle is coated on both poly (2-hydroxyethyl-methacrylate)-and polyethylene-glycol-methacrylate-grafted poly (methyl methacrylate), Int. J. Mol. Sci. 19 (9) (2018) 2764.

[43] A.M. Bakr, A. Darwish, A. Azab, M.E. El Awady, A.A. Hamed, A. Elzwawy, Structural, dielectric, and antimicrobial evaluation of PMMA/CeO_2 for optoelectronic devices, Sci. Rep. 14 (1) (2024) 2548.

[44] M. Khalifa, A.M. El Sayed, S.M. Kassem, E. Tarek, Synthesis, structural, optical, and thermal properties of $LaFeO_3$/poly (methyl methacrylate)/poly (vinyl acetate) nanocomposites for radiation shielding, Sci. Rep. 14 (1) (2024) 3672.

[45] L. Chang, E. Woo, Tacticity effects on glass transition and phase behavior in binary blends of poly(methyl methacrylate)s of three different configurations, Polym. Chem. 1 (2) (2010) 198–202.

[46] M.A. Forte, R.M. Silva, C.J. Tavares, R.F.e. Silva, Is poly (methyl methacrylate)(PMMA) a suitable substrate for ALD?: A review, Polymers 13 (8) (2021) 1346.

[47] J.D. Menczel, L. Judovits, R.B. Prime, H.E. Bair, M. Reading, S. Swier, Differential scanning calorimetry (DSC), in: J.D. Menczel, R.B. Prime (Eds.), Thermal Analysis of Polymers: Fundamentals and Applications, Wiley Online Library, Hoboken, 2009, pp. 7–239.

[48] J. Semen, J. Lando, The acid hydrolysis of isotactic and syndiotactic poly (methyl methacrylate), Macromolecules 2 (6) (1969) 570–575.

[49] N.A. Platé, A.D. Litmanovich, Y.V. Kudryavtsev, Theoretical considerations on the reactions in polymer blends, in: F. Ciardelli, S. Penczek (Eds.), Modification and Blending of Synthetic and Natural Macromolecules, Springer, Dordrecht, 2004, pp. 241–281.

[50] J. Kang, X. Li, Y. Zhou, L. Zhang, Supramolecular interaction enabled preparation of high-strength water-based adhesives from polymethylmethacrylate wastes, Iscience 26 (2) (2023).

[51] O.V. Chub, J.-L. Dubois, G.S. Patience, Zeolite Y hydrolyses methyl methacrylate to methacrylic acid in the gas phase, Chem. Eng. J. 459 (2023) 141479.

[52] Y. Kikuchi, M. Hirao, H. Sugiyama, S. Papadokonstantakis, K. Hungerbühler, T. Ookubo, A. Sasaki, Design of recycling system for poly (methyl methacrylate)(PMMA). part 2: process hazards and material flow analysis, Int. J. Life Cycle Assess. 19 (2014) 307–319.

[53] C. Martin, B. Haight, Devolatilization via twin-screw ExtrusionTheory, tips, and test results, in: I. Ghebre-Sellassie, C.E. Martin, F. Zhang, J. DiNunzio (Eds.), Pharmaceutical Extrusion Technology, CRC Press, Boca Raton, 2018, pp. 325–335.

[54] J. Cervantes-Uc, J. Cauich-Rodríguez, H. Vázquez-Torres, A. Licea-Claveríe, TGA/FTIR study on thermal degradation of polymethacrylates containing carboxylic groups, Polym. Degrad. Stab. 91 (12) (2006) 3312–3321.

[55] B.-C. Ho, Y.-D. Lee, W.-K. Chin, Thermal degradation of polymethacrylic acid, J. Polym. Sci. A 30 (11) (1992) 2389–2397.

[56] G. Cruciani, Zeolites upon heating: Factors governing their thermal stability and structural changes, J. Phys. Chem. Solids 67 (9–10) (2006) 1973–1994.